Microwave-assisted Synthesis of CuS/Graphene Composite for Enhanced Lithium Storage Properties

He Li, Yunhui Wang, Jingxin Huang, Yiyong Zhang, Jinbao Zhao*

State Key Laboratory of Physical Chemistry of Solid Surfaces, Collaborative Innovation Center of Chemistry for Energy Materials, State-Province Joint Engineering Laboratory of Power Source Technology for New Energy Vehicle, College of Chemistry and Chemical Engineering, Xiamen University, Xiamen 361005, China

ARTICLE INFO

ABSTRACT

In this work, CuS/graphene (CuS-G) composite is synthesized via one-pot microwave irradiation method under ambient conditions. As anode material for lithium ion batteries, the CuS-G composite delivers a significantly enhanced reversible capacity and charge/discharge cycle stability compared with pristine CuS. A capacity of 348 mAh g^{-1} can be maintained after 1000 cycles at the current density of 2.0 A g^{-1}. Electrochemical impedance spectroscopy (EIS) along with cyclic voltammetry (CV) and galvanostatic intermittent titration technique (GITT) measurements indicate that the incorporation of graphene sheets reduces the contact resistance and enhances lithium ion transfer rate during the electrochemical lithium insertion/extraction remarkably. Thus, as-prepared CuS spheres can be a promising anode material for high performance lithium ion batteries.

© 2016 Elsevier Ltd. All rights reserved.

1. Introduction

The rapid development of electric vehicles (EVs) and hybrid electric vehicles (HEVs) requires secondary batteries with higher power density [1–3]. Several key obstacles such as low power density, poor rate performance and insecurity are blocking the development of lithium ion batteries (LIBs). Researches on electrode materials with higher power density and safety are necessary and crucial.

Nowadays, graphite is still the most commonly used anode material for LIBs due to its low-cost and outstanding electrochemical performance. However, its lithiation potential (0.1 V vs. Li/Li$^+$) is close to the lithium stripping voltage, which may cause the formation and growth of lithium dendrite, leading to safety issues [4,5]. Li$_4$Ti$_5$O$_{12}$ (LTO) also draws much attention and has been successfully commercialized because of its higher operation voltage (1.5 V vs. Li/Li$^+$) and excellent cycle life. However, its theoretical capacity (175 mAh g^{-1}) and tapping density (1.64 g cm^{-3}) are not well satisfying the demand of power battery packs used in electric vehicles, not to mention its poor rate performances caused by poor electronic conductivity ($\sim 10^{-11}$ S m^{-1}) [6–8]. Therefore, substitutes of graphite or LTO anode materials are urgently called for. Metal sulfides are supposed to be next generation of electrode materials for secondary LIBs because of their high theoretical capacities and abundance [9–14]. Among them, CuS has drawn much attention due to its high theoretical capacity, flat voltage plateau and good electronic conductivity ($\sim 10^{-3}$ S cm^{-1}) [15–17]. Operation voltage of CuS (1.7 V vs. Li/Li$^+$) is in close proximity to that of LTO, which may sacrifice some energy density, but could avoid the formation of the lithium dendrite. Meanwhile, its theoretical capacity (560 mAh g^{-1}) is much greater than that of LTO and the mass density of CuS is up to 4.6 g cm^{-3} leading to much higher energy density than that of LTO. Therefore, CuS should be an ideal anode material for next-generation LIBs.

CuS usually suffer from poor cycling performance due to its volume change during lithiation/delithiation and loss of active material caused by dissolution of polysulfide [16,18]. Integrating CuS with carbon matrix like graphite, amorphous carbon or graphene is an optional way to solve these problems [19,20]. With outstanding chemical and electronic properties and mechanical strength, graphene could be an optimal compounding media for CuS. Firstly, the graphene sheets can cushion the volume changes during the charge and discharge due to its excellent mechanical strength. On the other hand, it can increase the electrical conductivity of the electrode, improve the rate performance of hybrid electrodes [21,22]. Tao et al. prepared CuS/graphene composite via one-pot hydrothermal method [23]. The CuS/graphene composite exhibits a relatively high reversible capacity and good cycling stability compared with bare CuS. Ren et al.

* Corresponding author. Tel.: +86 05922186935; fax: +86 05922186935.
E-mail address: jbzhao@xmu.edu.cn (J. Zhao).

synthesized "double-sandwich-like" CuS@reduced graphene oxide (rGO) used as an anode material in lithium ion batteries [24]. The "double-sandwich-like" CuS@rGO hybrids showed palpable improvement on capacity retention and rate performance than the CuS electrode. Feng et al. prepared CuS nanowires/rGO nanocomposites via a facile one-pot solution method in a mixed solvent of dimethyl sulfoxide (DMSO)-ethyl glycol (EG) [22]. The as-prepared CuSNWs/rGO nanocomposite revealed remarkable improvement in cycling stability as well as high-rate capability compared with pristine CuS nanowires. Although such progress has been made in preparing CuS/graphene (or rGO) composite, it is still a challenging work to develop a facile and low-cost method to prepare CuS/graphene composite.

Herein, we report a facile, ultrafast, low-cost and one-pot synthesis routine to fabricate CuS-G composite with the assistant of microwave irradiation. The CuS-G exhibits eminently enhanced electrochemical properties including excellent cycling stability and rate performance. Due to the convenience of preparing and remarkable lithium storage properties, the CuS-G shows great prospect for industrialized application as anode material for LIBs.

2. Experimental

2.1. Raw materials and synthesis

$Cu(NO_3)_2 \cdot H_2O$ (AR) and $Na_2S_2O_3 \cdot 5H_2O$ (AR) were purchased from Shanghai Chemical Co., Ltd. Graphene aqueous dispersion (3 wt.%) was purchased from Ningbo Material Technology and Engineering Institute. Acetylene black (battery grade), polypropylene fluorides (PVDF, battery grade) and N-methyl-2-pyrrolidene (NMP, battery grade) were purchased from Guangzhou Songbai Chemical Industrial Co., Ltd. Bis(trifluoromethane sulphonyl)imide (LiTFSI, battery grade), 1,2-Dimethoxyethane (DME, battery grade) and 1,3-dioxolane (DOL, battery grade) were bought from Zhangjiagang Guotai-Huarong New Chemical Materials Co., Ltd. All the chemicals were used without further purification.

In this work, CuS-G was prepared under microwave irritation, $Cu(NO_3)_2$ were used as copper source, $Na_2S_2O_3$ was used as a sulfur source, and deionized water was used as the solvent. In a typical synthesis procedure, 1.5 mL graphene aqueous dispersion was added into a 100 mL flat-bottom flask and treated with ultrasonic treatment for 1 h, then 20 mL 2.5 M $Cu(NO_3)_2$ solution and 20 mL 2.5 M $Na_2S_2O_3$ solution were added into the flask. The mixed solution was placed into the microwave reactor (Model: LWMC-201, microwave frequency: 2450 MHz, output power: 650 W, Nanjing Lingjiang Tech Corporation, P.R. China), and treated with microwave irritation pulse for 30 minutes under atmospheric conditions. Black powders were collected afterwards, washed by deionized water and anhydrous alcohol for several times followed by drying at 60 °C in the vacuum oven overnight.

For comparison, pristine CuS was prepared by the similar process in the absence of graphene aqueous dispersion.

2.2. Sample Characterization

The X-ray diffraction (XRD) patterns were recorded with Rigaku Miniflex 600 (Rigaku Corporation, Japan) with CuK_α radiation operated at 40 kV, 15 mA. The scanning rate is 2° min^{-1} and the scanning range is 10°–90° (2 theta). The Raman spectra were collected using a Renishaw spectrophotometer with a laser wavelength of 532 nm (Renishaw plc., UK). The elemental analysis was tested by Vario EL III Element Analyzer (Elementar Analysensysteme, Germany). The morphology and the elemental mapping were performed on the Hitachi S-4800 (Hitachi Corporation, Japan) scanning electron microscopy (SEM). Transmission electron microscopy (TEM) images and selected area
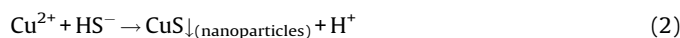
electron diffraction (SAED) pattern were tested on the JEM-2100 (JEOL, Japan) at 200 kV. The conductivity was measured by 4-probe conductivity measurements on ST-2722 semiconductor resistivity of the powder tester (Suzhou Jingge Electronic Co., Ltd., P.R. China).

2.3. Electrochemical measurement

The electrochemical characteristics were tested by CR2016-type coin cells. The active materials, acetylene black, and PVDF were mixed at the weight ratio of 80:10:10 in NMP. The slurry was coated on the copper foil and dried under vacuum oven at 60 °C for 12 hours. The loading of active materials on the electrodes is around 2.0–2.5 mg cm^{-2}. The electrode sheet was punched into 12 mm round discs, and pressed at 16 MPa to make an intimate contact between active materials and the current collector. The coin cells were assembled using the prepared electrodes as positive electrode and lithium metal as the negative electrode. The electrolyte was prepared by dissolving LiTFSI (1 mol L^{-1}) in the mixture solvent of DME and DOL (1:1, V/V). All cells were fabricated in an argon-filled glove box (M. Braun, Germany). The cyclic voltammetry (CV) curves were tested on the CHI 660D potentiostat (Shanghai Chenhua Instruments, P. R. China). The galvanostatically cycling measurements and galvanostatic intermittent titration technique (GITT) were carried out on the Neware CT-3008W battery test system (Neware Battery Testing Instruments, P.R. China). All the electrochemical tests were performed in the voltage range between 1.0 and 3.0 V. Electrochemical impendence spectroscopy (EIS) of CuS electrodes before and after 20 cycles were performed on the Autolab PGSTAT 101 (Metrohm Autolab, the Netherlands) in the frequency range from 0.01 Hz to 100 kHz using coin cells that lithium metal was used as the reference and counter electrode.

3. Results and discussion

As is known, microwave synthesis is a potent and alternative way to obtain inorganic material which owns the merits of time saving and high purity etc. [25–27]. Relying on the microwave-absorbing characteristic by substances, microwave synthesis takes advantage of "microwave dielectric heating" phenomena based on dipolar polarization or ionic conduction mechanism [26,28–30]. As polar molecules, water can be easily heated by microwave irradiation, high temperature can be generated, thus the reactions can take place rapidly. Compared with the common used hydrothermal method, the reaction time can be reduced from several hours to 30 minutes. Meanwhile, the purity and crystallinity of synthesized CuS are satisfying. The formation mechanism of CuS-G synthesized by microwave irradiation is shown in Fig. 1. The generation of CuS is based on a series of reactions between Cu^{2+} and $S_2O_3^{2-}$.

$$S_2O_3^{2-} + H_2O \rightarrow HS^- + HSO_4^- \tag{1}$$

$$Cu^{2+} + HS^- \rightarrow CuS\downarrow_{(nanoparticles)} + H^+ \tag{2}$$

The CuS nanoparticles will then aggregate into spherical shape, CuS spheres are formed eventually. As is reported before, the microwave absorbing abilities of most carbon materials are higher than that of distilled water [31]. With the presence of graphene sheets, the generated CuS are more likely to aggregate around the graphene sheets.

Fig. 2a shows XRD patterns of the CuS-G and pristine CuS. The diffraction pattern of CuS shows several strong diffraction lines around 30° (2 theta) along with a sharp diffraction line at 47.9°, the
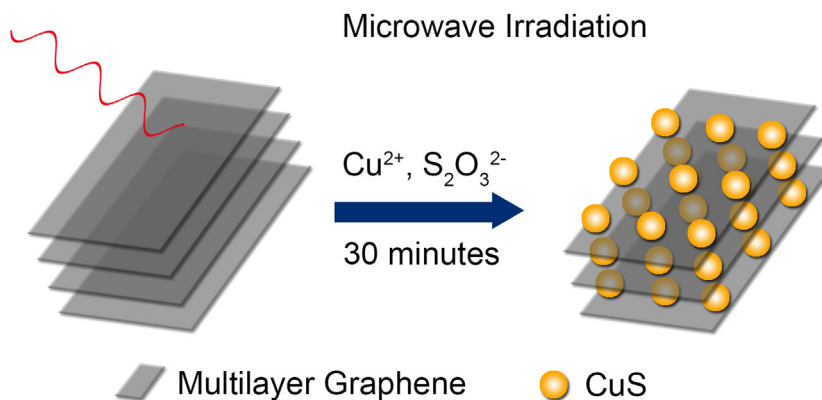
Microwave Irradiation

$Cu^{2+}, S_2O_3^{2-}$

30 minutes

Multilayer Graphene   CuS

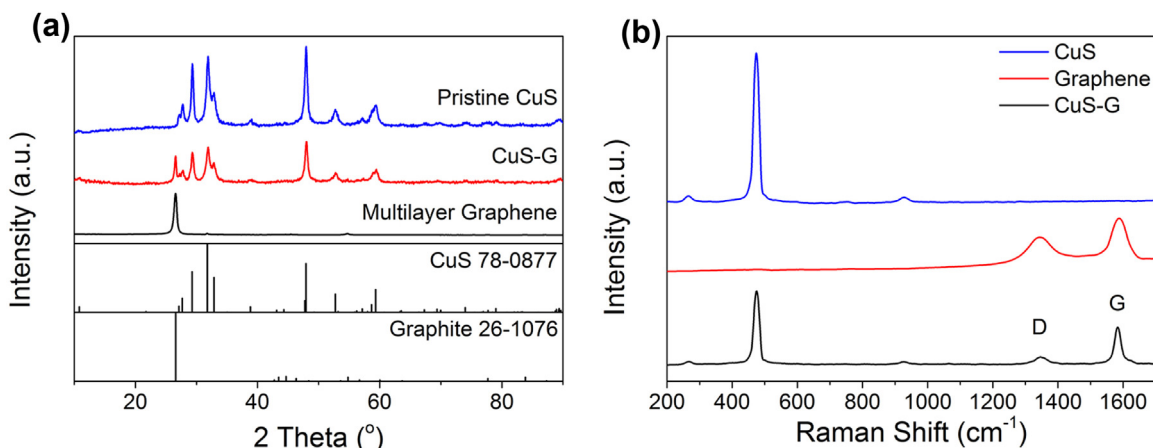**Fig. 1.** Schematic illustration of the formation of CuS-G.

Fig. 2. (a) XRD patterns, (b) Raman spectra of pristine CuS, graphene and CuS-G.

diffraction pattern corresponds well with the CuS standard card (JCPDS No. 78-0877). The CuS-G shows analogous pattern with pristine CuS, the difference lies in the diffraction line at 26.4° which belongs to the (002) plane of multilayer graphene. Both samples are further characterized by Raman spectroscopy (Fig. 2b). A strong Raman band at 474 cm^{-1} can be assigned to the S-S stretching mode of A_{1g} symmetry of CuS molecules as reported before [32]. The Raman bands of CuS-G at 1350 cm^{-1} and 1580 cm^{-1} are the characteristic D-band and G-band of graphene, respectively [33]. Wrapping by the graphene, the intensity of CuS becomes weaker. The weight ratio of graphene in the CuS-G composite is quantified to be 8.1% (Table S1, Supporting information).

Fig. 3 shows morphological information of CuS and CuS-G. Fig. 3a shows that the diameter of CuS spheres is about 800 nm, and the surface of CuS spheres is rough, indicating the CuS spheres are packed by primary nanoparticles. Fig. 3b displays the SEM image of CuS-G, graphene sheets can be observed, and the CuS spheres are distributed onto the surface of graphene or wrapped in the graphene sheets. TEM image of CuS-G are shown in Fig. 3c. Graphene sheets can be observed from the background. The SAED pattern (inset) and the high-resolution TEM (HR-TEM) image in Fig. 3d reveal that CuS spheres are polycrystalline, in other words, they are packed by primary particles in one direction or the other. From the HR-TEM image, several lattice fringes with the lattice spacing of 2.81, 3.05 and 3.22 Å can be observed, matching with (103), (102) and (101) planes of CuS (JCPDS No. 78-0877),

respectively. Fig. 4a–d demonstrate the SEM elemental mapping of CuS-G. Element C is distributed homogenously in the sight, the distribution of Cu and S is mainly concentrated on the spherical parts, indicating these are the CuS spheres.

Cyclic voltammetry (CV) was performed to figure out the lithium storage property of CuS-G electrode. The CV curves of CuS-G electrode are shown in Fig. 5a, which were carried out at the scan rate of 0.5 mV s^{-1} in the voltage range of 1.0 to 3.0 V. In the initial cathodic scan, two reduction peaks at 1.98 V and 1.45 V are observed, the peak at 1.98 V can be attributed to the phase transition from CuS to Cu_2S and the peak at 1.45 V can be attributed to the conversion reaction of Cu_2S to form Cu and Li_2S [16,34]. During the first anodic scan, two oxidation peaks are also observed, the oxidation peak at 1.95 V can be attributed to the oxidation of Cu and Li_2S to intermedia $Cu_{2-x}S$. The sharp oxidation peak at 2.41 V represents the over potential of Li_2S [35], this peak shrinks and vanishes in subsequent cycles. In the subsequent cycles, the reduction peak at higher potential vanishes gradually, this phenomenon will be explained in next part. The reduction peaks at lower potential shift to higher voltage, which indicates the energy barriers and the polarization of the electrodes decreases. The oxidation curves become more complicated, revealing complex reactions during the subsequent delithiation process [16].

Fig. 5b shows the voltage-capacity curves of the battery in different cycles at a current density of 0.2 A g^{-1}. The capacity of CuS-G composition is in respect of CuS only (similarly hereafter). It can be observed that larger polarization gaps exist in the first
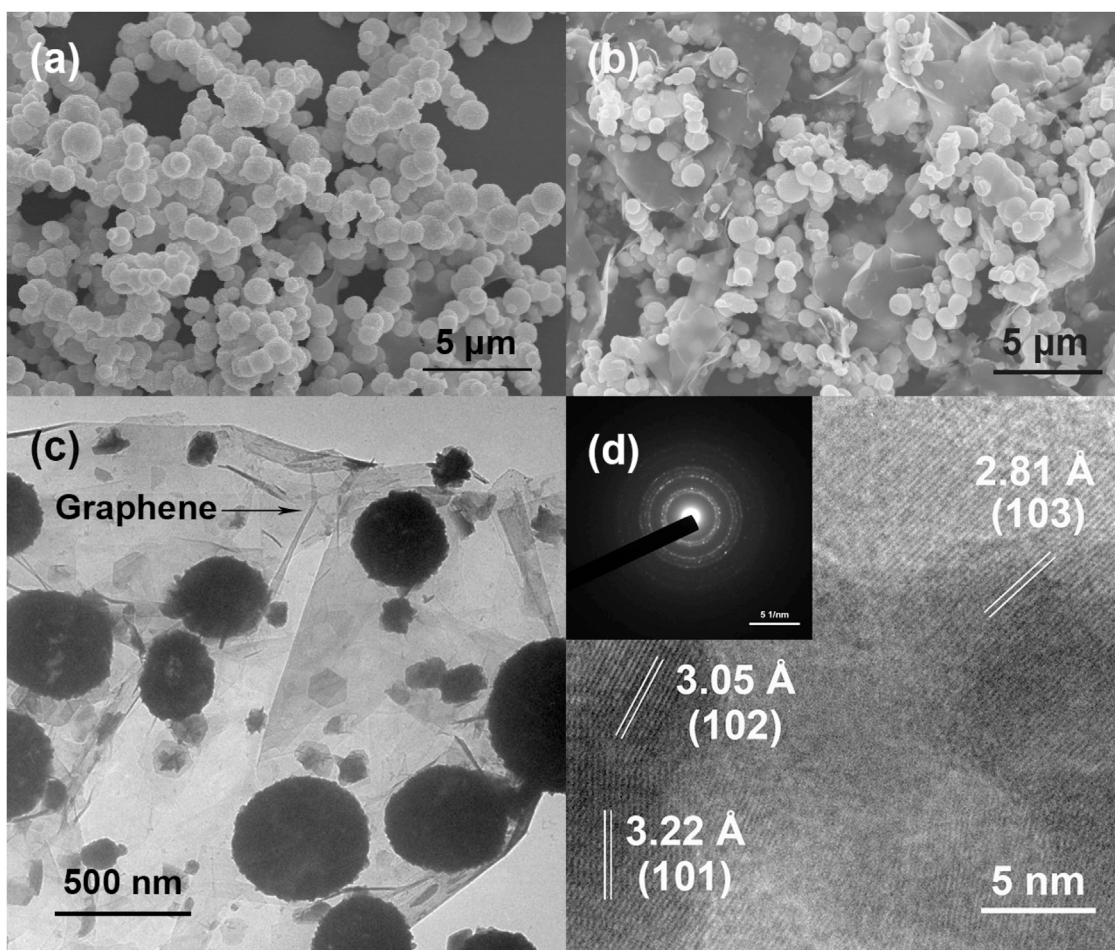
Fig. 3. (a) SEM image of pristine CuS, (b) SEM image, (c) TEM image, (d) HR-TEM image and SAED pattern (inset) of CuS-G.

several cycles, then the polarization decreases gradually, which indicates the activation of the active material. In the first cycle, there are two plateaus at around 2.0 V and 1.6 V. After several cycles, the plateau at 2.0 V disappears, only a plateau at 1.7 V can be seen. The charge-discharge curves match with the CV curves well. According to former reports by Tarascon et al. [36,37], the reactions taking place in the CuS electrode in the first lithiation could be described as:

$$2CuS + 2Li \rightarrow Cu_2S + Li_2S \tag{3}$$

$$Cu_2S + 2Li \rightarrow 2Cu + Li_2S \tag{4}$$

It also could be supported by Ex-situ XRD patterns and theoretical calculation which have been discussed in our previous works [16,18,38]. Similar with CuO, the reaction (3) is irreversible, during the subsequent lithiation process, reaction (4) becomes the major and highly reversible reaction, which explains the disappearance of the plateau at 2.0 V [39]. The initial discharge capacity is 627 mAh g^{-1} which surpasses the theoretical capacity of CuS (560 mAh g^{-1}). The extra capacity can be mainly due to the formation of solid electrolyte interface (SEI) and non-faradic storage. SEI can be formed from electrolyte solvent and electrolytic salt on the electrode surface, providing some extra capacity. As for the non-faradic storage mechanism, lithium ions could adhere to the surface of graphene due to negative charged groups on the

surface of graphene, leading to non-faradic capacity [22,24,40]. During the charge process, Cu and Li$_2$S are oxidized to Cu$_2$S or Cu$_{2-x}$S [38,41]. Combine with previous reports, the temporary oxidation potential may be caused by initial potential barriers of Li$_2$S which also vanishes after a few cycles [42,43]. Notably, CuS shows a long, flat discharge plateau, which suggests that batteries using CuS as electrodes could have a constant power output. It is very encouraging and makes CuS a probable material for commercial battery packs.

Fig. 5c shows cycle performances of pristine CuS and CuS-G at 0.2 A g^{-1} (0.36 C, 1 C = 0.56 A g^{-1}). For pristine CuS, a capacity of 379 mAh g^{-1} could be maintained after 100 cycles. For CuS-G, the capacity stands on 497 mAh g^{-1} after 100 cycles. To rule out the influence of graphene, a set of control experiments were conducted with graphene alone as the active material (Fig. S1). In the voltage range of 1.0-3.0 V, the capacity of graphene is less than 20 mAh g^{-1}, indicating the capacity of CuS-G is mainly contributed by CuS and the capacity of graphene can be ignored. CuS-G shows not only higher reversible capacity but also better cyclic performance. Long cycle performance at 2.0 A g^{-1} (3.6 C) is displayed in Fig. 5d. After 1000 cycles, the capacity remains at 348 mAh g^{-1}, and the columbic efficiency still maintains around 100%, exhibiting outstanding long cyclic performance.

The charge and discharge curves at different current densities are shown in Fig. 5e. The discharge capacities at current density of 0.2, 0.4, 0.8, 1.6, 2.0 and 4.0 A g^{-1} are 505, 440, 415, 383, 378 and

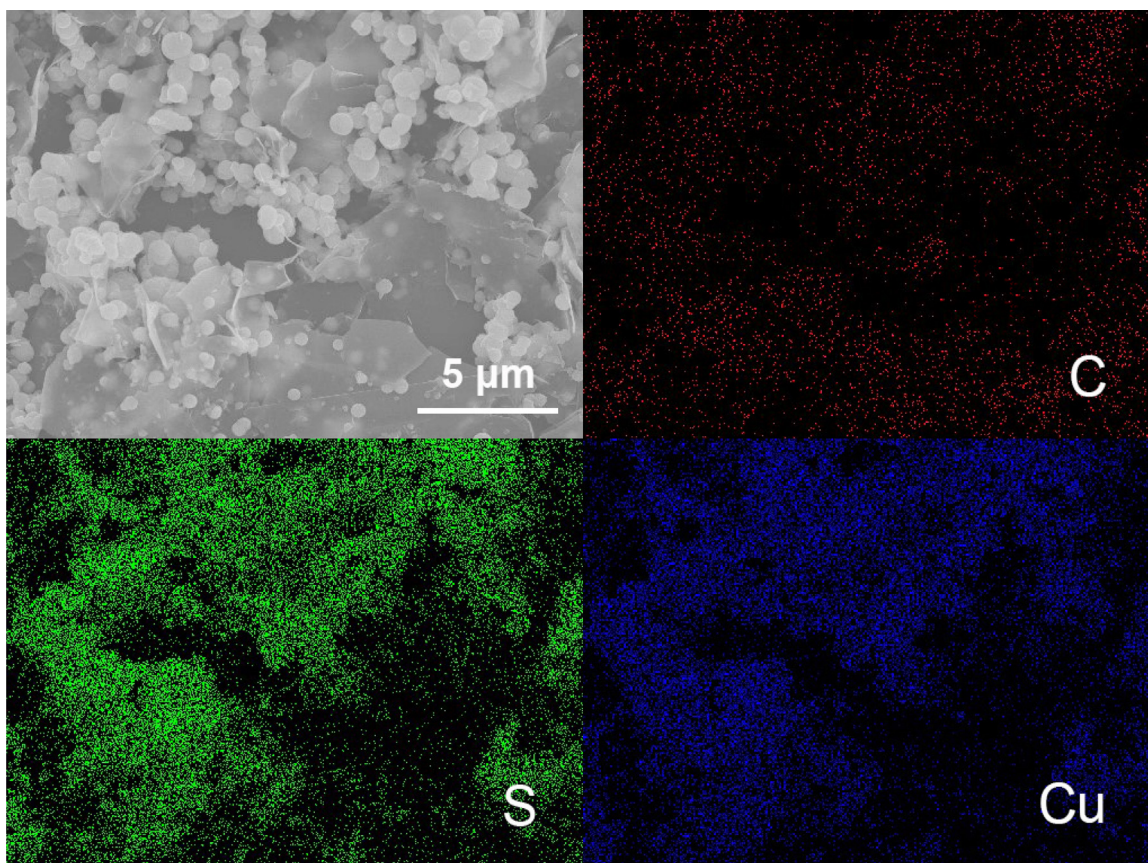**Fig. 4.** SEM elemental mapping of as-prepared CuS-G.

370 mAh g^{-1}, respectively. The coulombic efficiency keeps at approximately 100% even at high rates. The capacity can return to 442 mAh g^{-1} at the current density of 0.2 A g^{-1} (Fig. 5f).

Fig. 6 gives the distinct comparison of the rate capability of CuS-G in our work with CuS based materials reported before. These CuS based materials are prepared by other methods (hydrothermal method, solvothermal method etc.) [23,24,44,45]. All the counterparts are characterized under same/similar electrochemical measurement conditions. It can be seen that CuS-G exhibits high specific capacity and best rate property among these counterparts. Firstly, the CuS in our work shows regular spherical shape and uniform particle size which can make better contact between the active materials and electrolyte [46]. Secondly, the CuS spheres are distributed evenly around the graphene sheets, closely connecting to the conducting network provided by graphene sheets. The uniform size of CuS spheres, conducting network provided by graphene sheets makes the cycle stability and rate performance of our CuS-G sample better than other counterparts.

The electrochemical impedance spectra (EIS) of pristine CuS and CuS-G before and after 20 cycles are measured to investigate the electrode kinetics information. Fig. 7a shows the Nyquist plots before cycling, the semicircle at high frequencies is related to the charge-transfer resistance (R_{ct}) of the electrode and the slope at low frequencies stands for Warburg impendence (Z_w) of Li-ion diffusion [47]. The pristine CuS electrode shows larger semicircle than CuS-G electrode, meaning the CuS-G electrode has smaller charge-transfer resistance which can be attributed to the outstanding electronic conductivities of graphene sheets (Table 1). After 20 cycles (Fig. 7b), the R_{ct} of these batteries are obviously lower. The higher resistance observed from the fresh cells could be

due to the inactive surface film covering on the surface of electrode. The inactive surface film would be activated or decomposed as the charge-discharge progress carried out.

CV curves of CuS-G and pristine CuS at different scan rate from 0.1 to 1.0 mV s^{-1} are measured after 30 discharge-charge cycles at room temperature (Fig. 7c and Fig. S2). The lithium insertion and extraction peaks shift to lower and higher potential respectively as the scan rate increases. The CuS-G shows much smaller potential shift than that of pristine CuS, indicating decreased polarization and improved electrode kinetics. A good linear relationship (R^2 of CuS-G and CuS are 0.9983 and 0.9982, respectively) lies between the oxidation peak current (i_{pa}) and the square root of the scan rate ($v^{1/2}$) (Fig. 7d), demonstrating a diffusion-controlled process in the charge and discharge process. The lithium ion diffusion is the key factor to the electrode kinetics [48,49]. According to Randles–Sevcik Eq. (5), the apparent lithium ion diffusion coefficient (D_{app}) can be calculated:

$$i_{pa} = 0.4463nFAC\left(\frac{nFvD}{RT}\right)^{1/2} \qquad (5)$$

where n represents number of electrons transferred in the redox event, F is Faraday Constant, A is the working electrode area, C stands for lithium ion concentration, v is the scan rate, R is the gas constant and T is the temperature. From the slope of the linear fitting line in Fig. 7d, the apparent lithium ion diffusion coefficient of CuS-G is calculated to be 2.01×10^{-11} cm^2 s^{-1}, which is twice as large as that of pristine CuS (1.03×10^{-11} cm^2 s^{-1}).

The galvanostatic intermittent titration technique (GITT) is also carried out to provide further insight. Fig. 8a and Fig. S3 shows the GITT curves of CuS-G and pristine CuS at room temperature. The
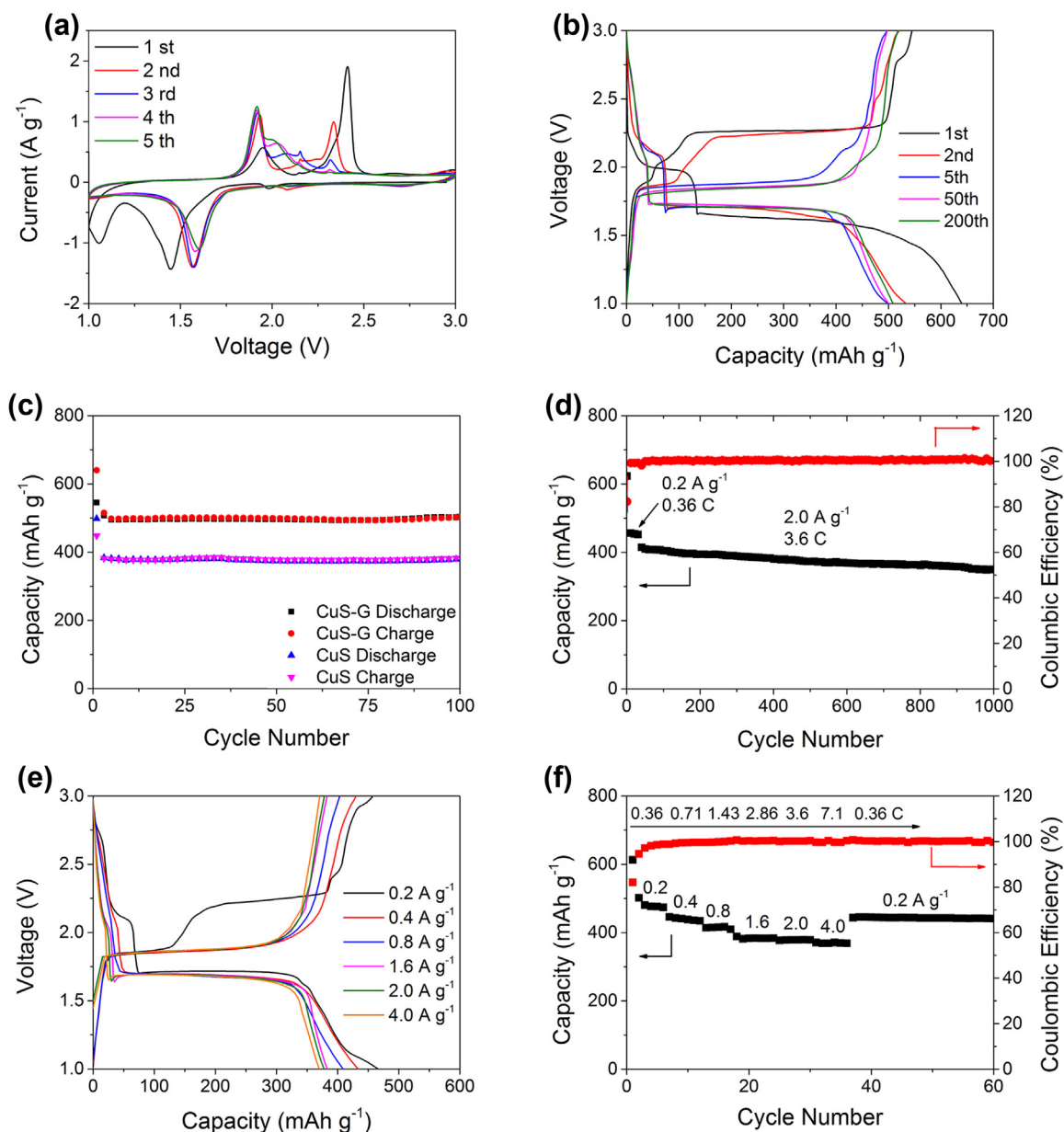
Fig. 5. (a) CV curves, (b) charge-discharge curves at $0.2\,A\,g^{-1}$, (c) cycle performance, (d) cycle performance at high current density, (e) charge-discharge curves at different current density, (f) rate performance of CuS-G electrode.

cells are the same cells used after the CV measurement. The cells are discharged at a constant current flux of 0.1C for an interval τ of 600 seconds followed by an open circuit standing for 3600 seconds to allow the cells relax to steady-state voltage (E_s). The GITT curves match well with the voltage-capacity curves tested previously. The specific discharge capacities of CuS-G and pristine CuS are calculated to be 450 and $440\,mAh\,g^{-1}$, matching with the charge-discharge cycle tests. The GITT data are used to determine the lithium ion diffusion coefficients (D_{Li}) in CuS-G and pristine CuS at various discharge states using the following formula:

$$D_{Li} = \frac{4}{\pi\tau}\left(\frac{m_B V_m}{M_B A}\right)^2 \left(\frac{\Delta E_s}{\Delta E_\tau}\right)^2 \left(\tau \ll L^2/D_{Li}\right) \qquad (6)$$

where V_m is the molar volume of the material, M_B and m_B are its molecular weight and active material mass, respectively, A is the

surface area of the electrode, L is the thickness of the electrode. ΔE_s is the steady-state voltage change after a current flux and open circuit standing, and ΔE_t is the voltage change during the constant current pulse, eliminating the iR drop [50–52]. Based on formula 6, the calculated D_{Li} of CuS-G and CuS at different discharge states are shown in Fig. 8b. D_{Li} of CuS-G lie between $3.51 \times 10^{-14}\,cm^2\,s^{-1}$ and $3.09 \times 10^{-11}\,cm^2\,s^{-1}$, while D_{Li} of CuS are in the range of $1.27 \times 10^{-14}\,cm^2\,s^{-1}$ to $1.98 \times 10^{-11}\,cm^2\,s^{-1}$. The calculated D_{Li} of CuS-G are also about two times larger than that of pristine CuS, which is in good agreement with the EIS and CV data, proving that the CuS-G composite enlarges the ion diffusion rate of the electrode, leading to better electrochemical performance. It can be concluded that the composite of CuS and graphene significantly reduces the contact resistance of the electrode and accelerate the transfer rate of lithium ions, the graphene sheets play an important
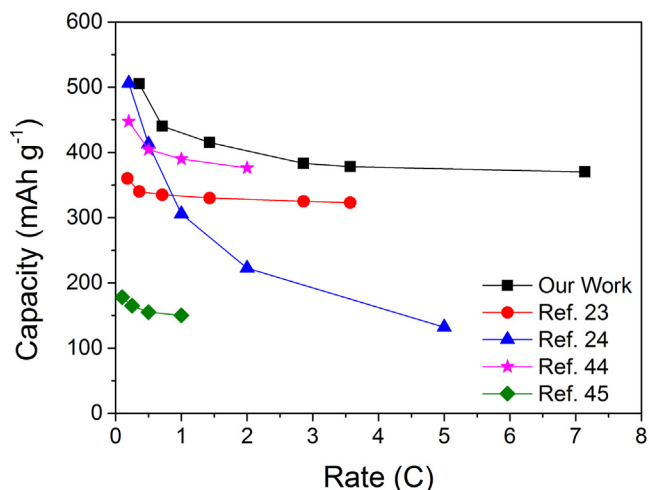
Fig. 6. Distinct comparison of the rate capability of CuS-G with CuS based materials reported before.

Table 1
Conductivities of pristine CuS, graphene and CuS-G determined by 4-probe conductivity measurements.

Sample	Specific resistance (Ω cm)	Specific conductivity (S cm^{-1})
CuS	0.024	42
Graphene	0.005	200
CuS-G	0.010	100

4. Conclusions

In summary, the CuS-G composite can be synthesized in short time (30 minutes) by a facile microwave irradiation method with simple raw materials under ambient condition. Electrochemical measurements reveal that as-prepared CuS-G shows good electrochemical performances compared with the pristine CuS. At the current density of 0.2 A g^{-1}, the CuS-G electrode shows discharge capacity of 497 mAh g^{-1} after 100 cycles. At the high current density of 2.0 A g^{-1}, 348 mAh g^{-1} can be maintained after 1000 cycles. The CuS-G electrode shows remarkable rate capability. At current density of 0.4, 0.8, 1.6, 2.0, and 4.0 A g^{-1}, 440, 415, 363, 361 and 350 mAh g^{-1} can be maintained, respectively. Meanwhile, the kinetic mechanism of CuS-G are explored using EIS, CV and GITT, revealing that the CuS-G shows improved kinetic properties which gives the composite better electrochemical performances. In consideration of the ultra-fast, low-cost synthetic method and the outstanding electrochemical performances of CuS-G, we believe that the microwave irradiation synthetic method could
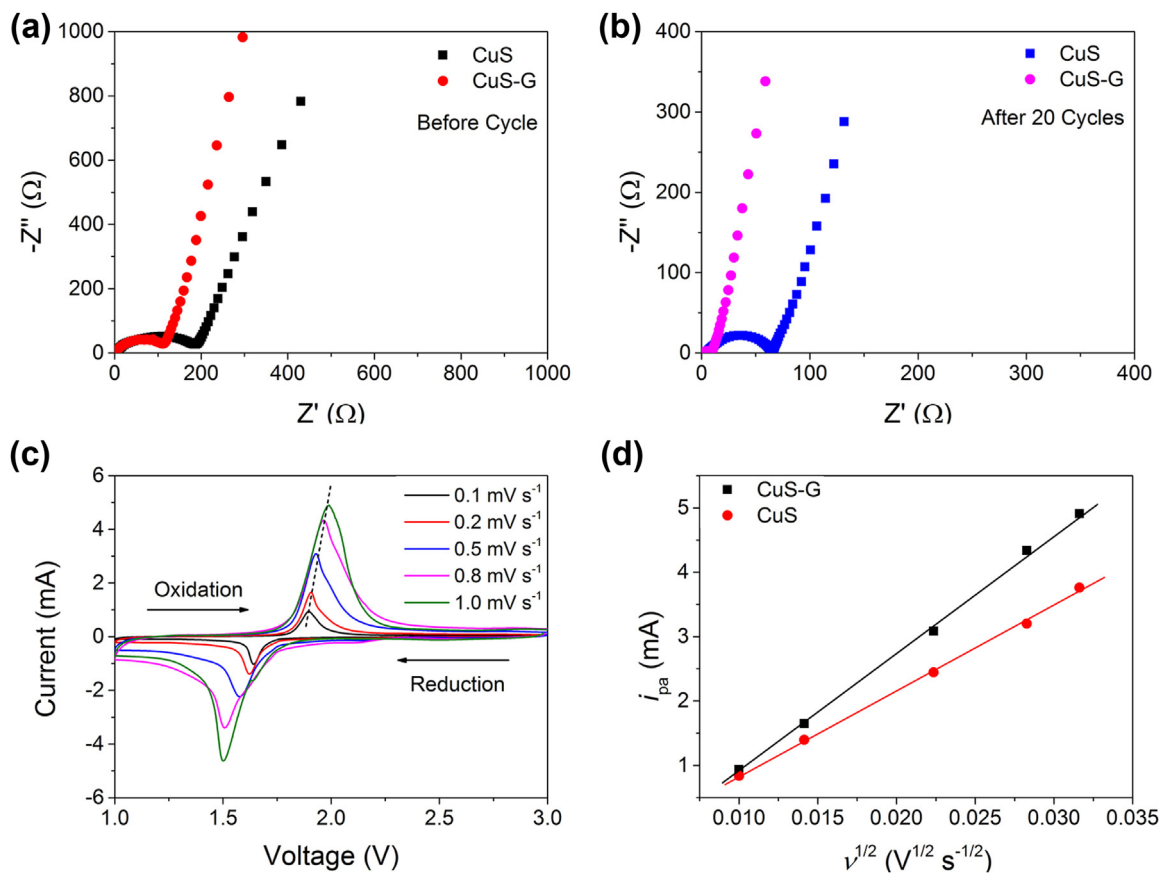
role in the enhancement of electrochemical performances of CuS. As-prepared CuS-G shows excellent electrochemical properties and great potential to be applied in the commercial battery packs.

Fig. 7. Nyquist plots of pristine CuS and CuS-G (a) before cycle and (b) after 20 cycles; (c) comparison of CV curves of CuS-G electrode at different scanning rate, (d) i_{pa}-$v^{1/2}$ scatters and fitting line of pristine CuS and CuS-G.
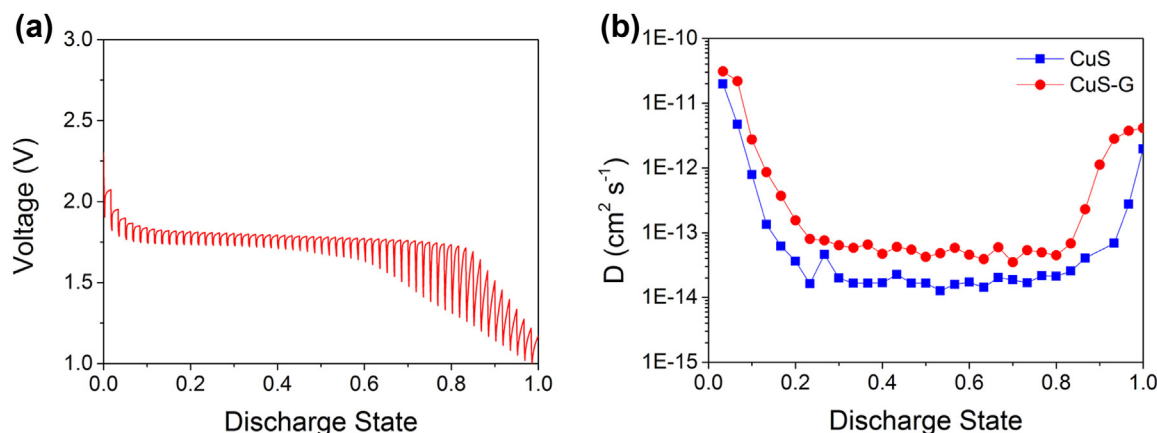
Fig. 8. (a) GITT curve of CuS-G electrode, (b) calculated diffusion coefficients of CuS-G and pristine CuS electrodes at different discharge states.

be applied to the industrialized preparation of copper sulfide and other metal sulfides, and as-prepared CuS-G composite could be suitable as the anode material for next-generation of commercial lithium-ion batteries.

Appendix A. Supplementary data

Supplementary data associated with this article can be found, in the online version, at http://dx.doi.org/10.1016/j.electacta.2016.12.117.

References

[1] M. Armand, J.M. Tarascon, Building better batteries, Nature 451 (2008) 652–657.
[2] P.G. Bruce, S.A. Freunberger, L.J. Hardwick, J.-M. Tarascon, Li-O₂ and Li-S batteries with high energy storage, Nat. Mater. 11 (2012) 19–29.
[3] J.B. Goodenough, Electrochemical energy storage in a sustainable modern society, Energ Environ Sci 7 (2014) 14–18.
[4] E. Peled, C. Menachem, D. Bar-Tow, A. Melman, Improved Graphite Anode for Lithium-Ion Batteries Chemically: Bonded Solid Electrolyte Interface and Nanochannel Formation, Journal of the Electrochemical Society 143 (1996) L4–L7.
[5] D. Aurbach, B. Markovsky, I. Weissman, E. Levi, Y. Ein-Eli, On the correlation between surface chemistry and performance of graphite negative electrodes for Li ion batteries, Electrochim Acta 45 (1999) 67–86.
[6] A. Ohzuku, Zero-Strain Insertion Material of Li [Li₁/₃Ti₅/₃] O₄ for Rechargeable Lithium Cells, Journal of the Electrochemical Society 142 (1995) 1431–1435.
[7] L. Zhao, Y.-S. Hu, H. Li, Z. Wang, L. Chen, Porous Li₄Ti₅O₁₂ Coated with N-Doped Carbon from Ionic Liquids for Li-Ion Batteries, Adv Mater 23 (2011) 1385–1388.
[8] J. Gao, C. Jiang, J. Ying, C. Wan, Preparation and characterization of high-density spherical Li₄Ti₅O₁₂ anode material for lithium secondary batteries, J Power Sources 155 (2006) 364–367.
[9] Z. Hu, K. Zhang, Z. Zhu, Z. Tao, J. Chen, FeS₂ microspheres with an ether-based electrolyte for high-performance rechargeable lithium batteries, J. Mater. Chem. A 3 (2015) 12898–12904.
[10] X. Rui, H. Tan, Q. Yan, Nanostructured metal sulfides for energy storage, Nanoscale 6 (2014) 9889–9924.
[11] S.-C. Han, K.-W. Kim, H.-J. Ahn, J.-H. Ahn, J.-Y. Lee, Charge–discharge mechanism of mechanically alloyed NiS used as a cathode in rechargeable lithium batteries, J Alloy Compd 361 (2003) 247–251.
[12] R. Jin, L. Yang, G. Li, G. Chen, Hierarchical worm-like CoS₂ composed of ultrathin nanosheets as an anode material for lithium-ion batteries, J Mater Chem A 3 (2015) 10677–10680.
[13] X. Fang, C. Hua, X. Guo, Y. Hu, Z. Wang, X. Gao, F. Wu, J. Wang, L. Chen, Lithium storage in commercial MoS₂ in different potential ranges, Electrochim Acta 81 (2012) 155–160.
[14] Y. Wang, X. Li, Y. Zhang, X. He, J. Zhao, Ether based electrolyte improves the performance of CuFeS₂ spike-like nanorods as a novel anode for lithium storage, Electrochim Acta 158 (2015) 368–373.
[15] Y. Chen, C. Davoisne, J.-M. Tarascon, C. Guéry, Growth of single-crystal copper sulfide thin films via electrodeposition in ionic liquid media for lithium ion batteries, J Mater Chem 22 (2012) 5295.
[16] X. Wang, Y. Wang, X. Li, B. Liu, J. Zhao, A facile synthesis of copper sulfides composite with lithium-storage properties, J Power Sources 281 (2015) 185–191.
[17] K. Sun, D. Su, Q. Zhang, D.C. Bock, A.C. Marschilok, K.J. Takeuchi, E.S. Takeuchi, H. Gan, Interaction of CuS and Sulfur in Li-S Battery System, Journal of the Electrochemical Society 162 (2015) A2834–A2839.
[18] C. Shi, X. Li, X. He, J. Zhao, New Insight into the Interaction between Carbonate-based Electrolyte and Cuprous Sulfide Electrode Material for Lithium Ion Batteries, Electrochim Acta 174 (2015) 1079–1087.
[19] S. Jiao, L. Xu, K. Jiang, D. Xu, Well-Defined Non-spherical Copper Sulfide Mesocages with Single-Crystalline Shells by Shape-Controlled Cu₂O Crystal Templating, Adv Mater 18 (2006) 1174–1177.
[20] W. Qiu, J. Jiao, J. Xia, H. Zhong, L. Chen, A self-standing and flexible electrode of yolk-shell CoS₂ spheres encapsulated with nitrogen-doped graphene for high-performance lithium-ion batteries, Chem. Eur. J. 21 (2015) 4359–4367.
[21] R. Mukkabla, P. Meduri, M. Deepa, P. Ghosal, Durable Li-S batteries with nano-sulfur/graphite nanoplatelets composites, Chemical Engineering Journal 303 (2016) 369–383.
[22] C. Feng, L. Zhang, M. Yang, X. Song, H. Zhao, Z. Jia, K. Sun, G. Liu, One-Pot Synthesis of Copper Sulfide Nanowires/Reduced Graphene Oxide Nanocomposites with Excellent Lithium-Storage Properties as Anode Materials for Lithium-Ion Batteries, ACS Appl Mater Interfaces 7 (2015) 15726–15734.
[23] H.-C. Tao, X.-L. Yang, L.-L. Zhang, S.-B. Ni, One-pot facile synthesis of CuS/graphene composite as anode materials for lithium ion batteries, Journal of Physics and Chemistry of Solids 75 (2014) 1205–1209.
[24] Y. Ren, H. Wei, B. Yang, J. Wang, J. Ding, Double-Sandwich-Like CuS@reduced graphene oxide as an Anode in Lithium Ion Batteries with Enhanced Electrochemical Performance, Electrochim Acta 145 (2014) 193–200.
[25] W. Qin, T. Chen, T. Lu, D.H.C. Chua, L. Pan, Layered nickel sulfide-reduced graphene oxide composites synthesized via microwave-assisted method as high performance anode materials of sodium-ion batteries, J Power Sources 302 (2016) 202–209.
[26] B.L. Cushing, V.L. Kolesnichenko, C.J. O'Connor, Recent Advances in the Liquid-Phase Syntheses of Inorganic Nanoparticles, Chemical Reviews 104 (2004) 3893–3946.
[27] J. Huang, A.C. Marschilok, E.S. Takeuchi, K.J. Takeuchi, Microwave-Assisted Synthesis of Silver Vanadium Phosphorus Oxide, Ag₂VO₂PO₄: Crystallite Size Control and Impact on Electrochemistry, Chemistry of Materials 28 (2016) 2191–2199.
[28] H.J. Kitchen, S.R. Vallance, J.L. Kennedy, N. Tapia-Ruiz, L. Carassiti, A. Harrison, A.G. Whittaker, T.D. Drysdale, S.W. Kingman, D.H. Gregory, Modern microwave methods in solid-state inorganic materials chemistry: from fundamentals to manufacturing, Chemical Reviews 114 (2014) 1170–1206.
[29] J. Liu, D. Xue, Rapid and scalable route to CuS biosensors: a microwave-assisted Cu-complex transformation into CuS nanotubes for ultrasensitive nonenzymatic glucose sensor, J. Mater. Chem. 21 (2011) 223–228.
[30] G.D. Stefanidis, A.N. Muñoz, G.S.J. Sturm, A. Stankiewicz, A helicopter view of microwave application to chemical processes: reactions, separations, and equipment concepts, Reviews in Chemical Engineering 30 (2014) 233–259.

[31] J.A. Menéndez, A. Arenillas, B. Fidalgo, Y. Fernández, L. Zubizarreta, E.G. Calvo, J. M. Bermúdez, Microwave heating processes involving carbon materials, Fuel Processing Technology 91 (2010) 1–8.

[32] B. Minceva-Sukarova, M. Najdoski, I. Grozdanov, C.J. Chunnilall, Raman spectra of thin solid films of some metal sulfides, Journal of Molecular Structure 410 (1997) 267–270.

[33] S. Reich, C. Thomsen, Raman spectroscopy of graphite, Philosophical Transactions of the Royal Society of London. Series A: Mathematical, Physical and Engineering Sciences 362 (2004) 2271–2288.

[34] A. Débart, L. Dupont, R. Patrice, J.M. Tarascon, Reactivity of transition metal (Co, Ni, Cu) sulphides versus lithium: The intriguing case of the copper sulphide, Solid State Sci 8 (2006) 640–651.

[35] Y. Yang, G. Zheng, S. Misra, J. Nelson, M.F. Toney, Y. Cui, High-capacity micrometer-sized Li_2S particles as cathode materials for advanced rechargeable lithium-ion batteries, J Am Chem Soc 134 (2012) 15387–15394.

[36] C.-H. Lai, K.-W. Huang, J.-H. Cheng, C.-Y. Lee, B.-J. Hwang, L.-J. Chen, Direct growth of high-rate capability and high capacity copper sulfide nanowire array cathodes for lithium-ion batteries, J Mater Chem 20 (2010) 6638–6645.

[37] Y. Chen, C. Davoisne, J.-M. Tarascon, C. Guéry, Growth of single-crystal copper sulfide thin films via electrodeposition in ionic liquid media for lithium ion batteries, J Mater Chem 22 (2012) 5295–5299.

[38] X. Li, X. He, C. Shi, B. Liu, Y. Zhang, S. Wu, Z. Zhu, J. Zhao, Synthesis of one-dimensional copper sulfide nanorods as high-performance anode in lithium ion batteries, ChemSusChem 7 (2014) 3328–3333.

[39] X. Wang, D.-M. Tang, H. Li, W. Yi, T. Zhai, Y. Bando, D. Golberg, Revealing the conversion mechanism of CuO nanowires during lithiation-delithiation by in situ transmission electron microscopy, Chem Commun 48 (2012) 4812–4814.

[40] F. Klein, B. Jache, A. Bhide, P. Adelhelm, Conversion reactions for sodium-ion batteries, Phys Chem Chem Phys 15 (2013) 15876–15887.

[41] B. Jache, B. Mogwitz, F. Klein, P. Adelhelm, Copper sulfides for rechargeable lithium batteries: Linking cycling stability to electrolyte composition, J Power Sources 247 (2014) 703–711.

[42] L. Wang, Y. Wang, Y. Xia, A high performance lithium-ion sulfur battery based on a Li_2S cathode using a dual-phase electrolyte, Energ Environ Sci 8 (2015) 1551–1558.

[43] J. Hassoun, B. Scrosati, A high-performance polymer tin sulfur lithium ion battery, Angewandte Chemie 49 (2010) 2371–2374.

[44] Y. Wang, X. Zhang, P. Chen, H. Liao, S. Cheng, In situ preparation of CuS cathode with unique stability and high rate performance for lithium ion batteries, Electrochim Acta 80 (2012) 264–268.

[45] J. Cheng, Y. Pan, J. Zhu, Z. Li, J. Pan, Z. Ma, Hybrid network CuS monolith cathode materials synthesized via facile in situ melt-diffusion for Li-ion batteries, J Power Sources 257 (2014) 192–197.

[46] B. Li, Y. Yu, J. Zhao, Facile synthesis of spherical $xLi_2MnO_3\cdot(1-x)Li$ $(Mn_{0.33}Co_{0.33}Ni_{0.33})O_2$ as cathode materials for lithium-ion batteries with improved electrochemical performance, J Power Sources 275 (2015) 64–72.

[47] F. Nobili, S. Dsoke, F. Croce, R. Marassi, An ac impedance spectroscopic study of Mg-doped $LiCoO_2$ at different temperatures: electronic and ionic transport properties, Electrochim Acta 50 (2005) 2307–2313.

[48] Z. Hu, Z. Zhu, F. Cheng, K. Zhang, J. Wang, C. Chen, J. Chen, Pyrite FeS_2 for high-rate and long-life rechargeable sodium batteries, Energ Environ Sci 8 (2015) 1309–1316.

[49] Y. Yang, J. Li, X. He, J. Wang, D. Sun, J. Zhao, A facile spray drying route for mesoporous Li_3VO_4/C hollow spheres as an anode for long life lithium ion batteries, J. Mater. Chem. A 4 (2016) 7165–7168.

[50] K.M. Shaju, G.V. Subba Rao, B.V.R. Chowdari, Influence of Li-Ion Kinetics in the Cathodic Performance of Layered $Li(Ni_{1/3}Co_{1/3}Mn_{1/3})O_2$, Journal of the Electrochemical Society 151 (2004) A1324.

[51] Y. You, H.R. Yao, S. Xin, Y.X. Yin, T.T. Zuo, C.P. Yang, Y.G. Guo, Y. Cui, L.J. Wan, J.B. Goodenough, Subzero-Temperature Cathode for a Sodium-Ion Battery, Adv Mater 28 (2016) 7243–7248.

[52] Z. Shen, L. Cao, C.D. Rahn, C.Y. Wang, Least Squares Galvanostatic Intermittent Titration Technique (LS-GITT) for Accurate Solid Phase Diffusivity Measurement, Journal of the Electrochemical Society 160 (2013) A1842–A1846.